ATLAS CONF Note

ATLAS-CONF-2018-054

November 29, 2018

Combination of searches for invisible Higgs boson decays with the ATLAS experiment

The ATLAS Collaboration

Dark matter particles, if sufficiently light, may be produced in decays of the Higgs boson. This document presents a statistical combination of searches for the resulting $H \to$ invisible (inv) decays where H is produced according to the Standard Model via vector boson fusion, $Z(\ell\ell)H(\text{inv})$, and $W/Z(\text{had})H(\text{inv})$, all performed with the ATLAS detector using 36.1 fb^{-1} of pp collisions at a center-of-mass energy of $\sqrt{s} = 13$ TeV at the LHC. In combination with the results at $\sqrt{s} = 7$ and 8 TeV, an exclusion limit on the $H \to$ inv branching ratio of $\mathcal{B}_{H\to\text{inv}} < 0.26$ ($0.17^{+0.07}_{-0.05}$) at 95% confidence level is observed (expected).

One of the central open questions in physics today is the nature of dark matter (DM) that is found to comprise most of the matter in the universe [1–6]. A compelling candidate for DM is a stable electrically neutral particle χ whose non-gravitational interactions with Standard Model (SM) particles are weak. Such a particle could be detectable at the scale of electroweak symmetry breaking [7–9] and accommodate the observed DM relic density [10, 11]. Many models predict detectable production rates of such DM particles at the Large Hadron Collider (LHC) [12]. In a wide class of those models, the 125 GeV Higgs boson H [13, 14] acts as a portal between the dark sector and the SM sector, either through Yukawa-type couplings to fermionic dark matter, or other mechanisms [15–28]. If kinematically allowed, decays of the Higgs boson to DM particles represent a distinct signature in such models. Higgs boson decays to DM particles can only be indirectly inferred through missing transverse momentum[1] $E_{\mathrm{T}}^{\mathrm{miss}}$ due to DM particles escaping detection, and are therefore termed "invisible".

Direct searches for invisible Higgs boson decays have been carried out at ATLAS in Run 1 of the LHC, using up to 4.7 fb^{-1}of pp collision data at a center-of-mass energy of $\sqrt{s}$ = 7 TeV and up to 20.3 fb^{-1} at 8 TeV. Different event topologies were considered, assuming SM production rates: vector boson fusion (VBF) [29], Higgsstrahlung from a Z boson decaying into charged leptons (ZH) [30], and Higgsstrahlung from a W or Z boson decaying into hadrons (VH) [31]. These searches for invisible Higgs boson decays have been statistically combined, and an upper limit at 95% confidence level (CL) on the invisible Higgs boson branching ratio of $\mathcal{B}_{H\to\mathrm{inv}} < 0.25\ (0.27^{+0.10}_{-0.08})$ [32] was observed (expected). In combination with visible decay modes of the Higgs boson, the upper observed (expected) limit improves to 0.23 (0.24) [32]. Direct searches for invisible Higgs decays have been performed using up to 36.1 fb^{-1} of pp collision data at $\sqrt{s}$ = 13 TeV recorded in 2015 and 2016 in the VBF [33], ZH [34], and VH [35] topologies with the ATLAS detector [36–38]. The aforementioned results at $\sqrt{s}$ = 13 TeV will be referred to as "Run 2 results" in the following. Similar searches have been performed by the CMS Collaboration [39–43].

This document presents the statistical combination of the Run 2 searches for invisible decays of the 125 GeV Higgs boson using the ATLAS detector. Subsequently, a statistical combination with the combined Run 1 result [32] from ATLAS is performed. An overview of all results used as input in this combination is given in Table 1. The analysis is performed under the assumption of SM Higgs boson production. Visible decay modes of the 125 GeV Higgs boson are not considered.

A brief overview of the Run 2 searches for $H \to$ inv is given below.

- **VBF topology [33]:** The analysis of the VBF production mode employs a $E_{\mathrm{T}}^{\mathrm{miss}}$ trigger that is 98% efficient or better in the considered region of phase space. The event selection requires $E_{\mathrm{T}}^{\mathrm{miss}} > 180$ GeV. Jets (j) are reconstructed up to $|\eta(j)| < 4.5$ from energy clusters in the calorimeter using the anti-k_t algorithm [44] with a radius parameter $R = 0.4$. The selected events require two jets leading in p_{T} to be separated by $|\Delta\eta_{jj}| > 4.8$. There should be no additional jets with $p_{\mathrm{T}} > 25$ GeV and no isolated electron or muon candidate with $p_{\mathrm{T}} > 7$ GeV. These requirements serve to reduce the contribution from W/Z production in association with jets (V+jets). In the search signal region (SR) the m_{jj} distribution of the background falls more rapidly than the signal, where m_{jj} represents the invariant mass of the two selected leading jets. Thus the SR is divided into three m_{jj} regions ($1 < m_{jj}/\mathrm{TeV} < 1.5$, $1.5 < m_{jj}/\mathrm{TeV} < 2$, $m_{jj}/\mathrm{TeV} > 2$) to improve the

[1] ATLAS uses a right-handed coordinate system with its origin at the nominal interaction point (IP) in the center of the detector and the z-axis along the beam pipe. The x-axis points to the center of the LHC ring, and the y-axis points upward. Cylindrical coordinates (r, ϕ) are used in the transverse plane, ϕ being the azimuthal angle around the z-axis. The pseudorapidity is defined in terms of the polar angle θ as $\eta = -\ln\tan(\theta/2)$. The distance between two objects in η–ϕ space is $\Delta R = \sqrt{(\Delta\eta)^2 + (\Delta\phi)^2}$. Transverse momentum is defined by $p_{\mathrm{T}} = p\sin\theta$.

search sensitivity. The dominant background sources are $Z(\nu\nu)$ + jets and $W(\ell\nu)$ + jets production, where the charged lepton ℓ is not detected. Control regions (CR) enriched in these processes are defined to determine their normalization factors in the SR. The main uncertainty contributors are the finite number of simulated Monte Carlo (MC) events, the modelling of V +jets production, and the uncertainty from the jet energy scale (JES). The final discriminant is the number of events in the three m_{jj} regions.

- ***ZH* topology [34]:** This search is conducted in the Higgsstrahlung channel where the Z boson decays into a pair of electrons or muons. A selected candidate event must pass at least one of the various single-lepton triggers, fulfill $E_{\mathrm{T}}^{\mathrm{miss}} > 90$ GeV and $E_{\mathrm{T}}^{\mathrm{miss}}/H_T > 0.6$, where H_T is calculated as the scalar sum of the p_{T} of the selected leptons and jets, and have exactly one pair of isolated electrons or muons with an invariant mass that is consistent with that of the Z boson. The transverse momentum requirement on the leading (subleading) charged lepton is $p_{\mathrm{T}} > 30$ (20) GeV. To reduce the Z+jets background, the dilepton system must be aligned back-to-back relative to the $E_{\mathrm{T}}^{\mathrm{miss}}$ vector in the transverse plane. Events with jets originated by b quarks (b-jets) are vetoed to suppress backgrounds from top quark pair ($t\bar{t}$) production and W boson production in association with a single top quark (Wt). The irreducible $Z(\nu\nu)Z(\ell\ell)$ background is estimated from MC simulations and its production yield is normalized to the theoretical prediction. The $W(\ell\nu)Z(\ell\ell)$ background contribution is also predicted with MC simulations and is normalized by a scale factor that is obtained from a CR enriched in WZ events. The Z+jets background is estimated with a data-driven method that uses Z-enriched regions that are disjoint from the SR. The final discriminant is $E_{\mathrm{T}}^{\mathrm{miss}}$.
- ***VH* topology [35]:** This analysis considers the Higgsstrahlung channel where the associated W or Z boson decays into hadrons. The final state signature of large $E_{\mathrm{T}}^{\mathrm{miss}}$ and jets also receives contributions from Higgs boson production via gluon fusion with jets originating from initial state radiation, and production via the VBF process. For growing V boost, the two jets from its decay become increasingly collimated, and are eventually merged into one single reconstructed jet. Thus, this search is conducted in two topological channels. In the "merged" topology, the SR is defined with $E_{\mathrm{T}}^{\mathrm{miss}} > 250$ GeV and has at least one trimmed [45, 46] large-R jet (J) that is reconstructed using the anti-k_t algorithm with $R = 1.0$. The signal large-R jet is the one with the highest p_{T}. For the "resolved" topology, the selected event should have $E_{\mathrm{T}}^{\mathrm{miss}} > 150$ GeV and at least two small-R jets (j) with $R = 0.4$. Selected events must pass a $E_{\mathrm{T}}^{\mathrm{miss}}$ trigger and must not contain an isolated electron or muon with $p_{\mathrm{T}} > 7$ GeV. Each event is first passed through the merged topology selection and, if it fails, it is passed through the resolved topology selection. To improve the search sensitivity, the selected events are further split into categories with zero, one, and two identified b-jets, and into two mass regions of the invariant mass of the signal large-R jet (two signal small-R jets) for the merged (resolved) topology. The low mass region ($70 \lesssim m_J, m_{jj}/\mathrm{GeV} \lesssim 100$) targets the hadronic W/Z boson decays of the associated production, whereas the high mass region ($100 \lesssim m_J, m_{jj}/\mathrm{GeV} < 250$) is optimized for gluon fusion and VBF production. The main background contributions are from the V +jets and $t\bar{t}$ processes. The predictions from MC simulations are constrained with CRs that contain one or two leptons, and are kinematically similar to the SR. The final discriminant is $E_{\mathrm{T}}^{\mathrm{miss}}$.

The SRs and CRs of the individual input analyses are either orthogonal by construction, or were shown to have an overlap below 1%, which is neglected in the following.

The statistical combination of the individual analyses is performed by maximizing the combined binned likelihood ratio $\Lambda(\mathcal{B}_{H\to\mathrm{inv}};\theta)$ [47] following the implementation described in Ref. [48, 49], with $\mathcal{B}_{H\to\mathrm{inv}}$ as the parameter of interest. Systematic uncertainties are modeled in the likelihood function as nuisance parameters θ constrained by Gaussian or log-normal probability density functions [32].

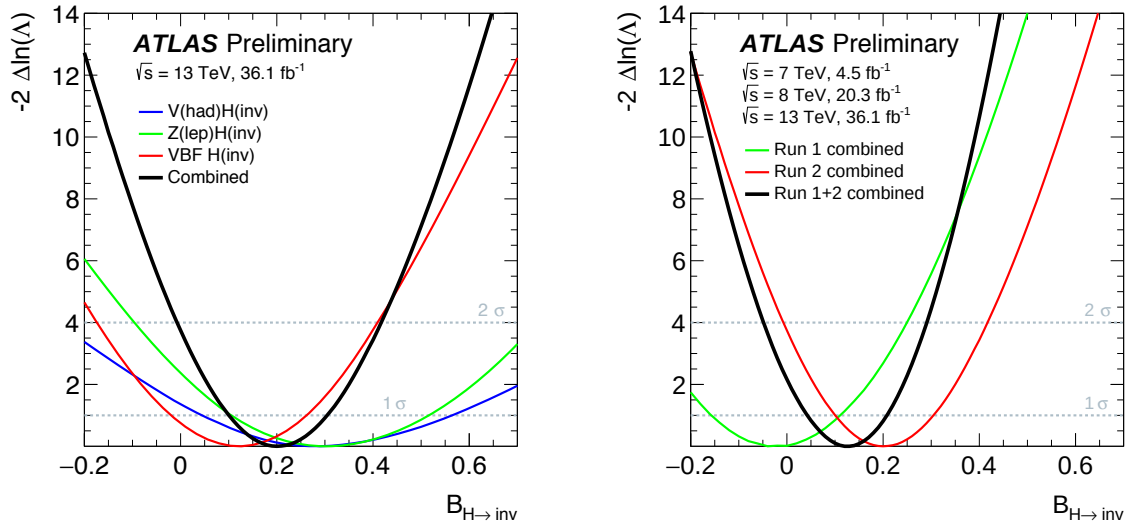

Figure 1: The observed negative logarithmic profile likelihood ratios $-2\,\Delta\ln(\Lambda)$ as a function of $\mathcal{B}_{H\to\text{inv}}$ of the VH, ZH, and VBF topologies using Run 2 data only and their statistical combination (left). The latter, together with the corresponding function of the Run 1 combination, and their total Run 1+2 combination (right).

In the combination of Run 2 results, the experimental systematic uncertainties as well as the uncertainty on the integrated luminosity and the modeling of additional pp collisions in the same and neighboring bunch crossings (pile-up) are correlated across all search channels. Some experimental uncertainties related to flavor tagging and the JES are represented through different parameterizations in the input analyses and are therefore treated as uncorrelated. The impact of this assumption on the combined result is estimated using alternative correlation models where the leading sources of systematic uncertainty in the respective parameterizations are treated as correlated, and found to have an absolute effect on the $\mathcal{B}_{H\to\text{inv}}$ limit of $O(0.01)$. The systematic uncertainties on the total $H\to$ inv signal cross section due to the choice of parton distribution functions (PDF) are considered correlated between all channels, and due to missing higher order corrections, estimated through variation of factorization and renormalisation scales, are treated as correlated between the ZH and VH processes, but not with VBF. The impact of the corresponding uncertainties on the acceptance rather than the total cross section of VH production is evaluated and found negligible. Few systematic uncertainties that are tightly constrained in a given analysis are left uncorrelated in order not to introduce any potential phase space specific biases.

The negative logarithmic profile likelihood ratios $-2\,\Delta\ln(\Lambda)(\mathcal{B}_{H\to\text{inv}};\theta)$ as a function of $\mathcal{B}_{H\to\text{inv}}$ of the combined Run 2 result and the individual analyses are shown in Fig. 1. The dominant uncertainty sources are finite event yields in data and MC, reconstruction of jets and leptons, and modelling of diboson and W/Z + jets production. In absence of a significant excess, an upper limit at 95% CL of $\mathcal{B}_{H\to\text{inv}} < 0.38$ $(0.21^{+0.08}_{-0.06})$ is observed (expected) with the CL_s formalism [50], using the profile likelihood ratio as a test statistic. The excess in data corresponds to a p_{SM}-value of 3% under the SM hypothesis of $\mathcal{B}_{H\to\text{inv}} \simeq 10^{-3}$, and is a consequence of the excesses present in each of the three input analyses.

Subsequently, the above Run 2 result is combined with the Run 1 searches for $H\to$ inv decays [32]. Due to the changes in the detector layout and conditions, the reconstruction algorithms and their calibrations, as well as differences in the treatment of systematic uncertainties, the correlations between them are not

Table 1: Observed and expected upper limits on $\mathcal{B}_{H\to\text{inv}}$ at 95% CL from direct searches for invisible decays of the 125 GeV Higgs boson and statistical combinations. Also given are the observed p-values under the SM hypothesis.

Analysis	$\sqrt{s}$	Int. luminosity	Observed	Expected	p_{SM}-value	Reference
Run 2 VBF	13 TeV	36.1 fb^{-1}	0.37	$0.28^{+0.11}_{-0.08}$	0.19	[33]
Run 2 ZH	13 TeV	36.1 fb^{-1}	0.67	$0.39^{+0.17}_{-0.11}$	0.06	[34]
Run 2 VH	13 TeV	36.1 fb^{-1}	0.83	$0.58^{+0.23}_{-0.16}$	0.12	[35]
Run 2 Comb.	13 TeV	36.1 fb^{-1}	0.38	$0.21^{+0.08}_{-0.06}$	0.03	this note
Run 1 Comb.	7, 8 TeV	4.7, 20.3 fb^{-1}	0.25	$0.27^{+0.10}_{-0.08}$	—	[32]
Run 1+2 Comb.	7, 8, 13 TeV	4.7, 20.3, 36.1 fb^{-1}	0.26	$0.17^{+0.07}_{-0.05}$	0.10	this note

clearly identifiable. Hence, no correlations between Run 1 and 2 are assumed for most instrumental uncertainties. The uncertainties related to the modeling of the calorimeter response dependence on jet flavor and pile-up are taken as either correlated or uncorrelated between the runs, and the choice which results in a weaker expected exclusion limit on $\mathcal{B}_{H\to\text{inv}}$ is adopted. The uncertainty on the b-JES is estimated using MC simulations [51, 52] and is therefore considered correlated. For the signal modeling, the parton shower uncertainty in the VH channel, the uncertainty from missing higher order corrections in the ZH analysis, and the uncertainty on the jet multiplicity in the VBF channel [53] are each taken as correlated between the runs, since the estimated uncertainties stem from the same source. For the same reason, the uncertainty from missing higher order corrections on the dominant background from diboson production in the ZH search is treated as correlated. All other background modeling uncertainties are considered uncorrelated. The impact of these correlation assumptions on the combined $\mathcal{B}_{H\to\text{inv}}$ limit is found to be at most 0.005. In addition, scenarios ranging from full anti-correlation to full correlation were studied using BLUE [54] for the components of the JES uncertainty, the V+jets background, and the diboson production that are nominally not correlated due to different parameterisations in Run 1 and 2. Their absolute effect on the $\mathcal{B}_{H\to\text{inv}}$ limit is at most 0.01.

The observed $-2\,\Delta\ln(\Lambda)(\mathcal{B}_{H\to\text{inv}};\theta)$ ratio of the combined Run 1+2 result is represented in Fig. 1 alongside the individual Run 1 and Run 2 combinations. An upper limit of $\mathcal{B}_{H\to\text{inv}} < 0.26$ ($0.17^{+0.07}_{-0.05}$) at 95% CL is observed (expected). The p_{SM}-value under the SM hypothesis is 10%. The final result, together with the results in the individual Run 2 analyses as well as the Run 2-only and the Run 1-only combinations, is summarized in Table 1, and the upper limits on $\mathcal{B}_{H\to\text{inv}}$ are graphically represented in Fig. 2.

The combined observed Run 1+2 exclusion limit of $\mathcal{B}_{H\to\text{inv}} < 0.24$ at 90% CL is shown together with the limits from representative direct DM detection experiments [55–59] in Fig. 3. This comparison is performed in the context of Higgs portal models [60]. The translation of the $H \to$ inv result into a weak interacting massive particle–nucleon scattering cross section $\sigma_{\text{WIMP-}N}$ is performed in an effective field theory approach [29] under the assumption that invisible Higgs decays to a pair of WIMPs are kinematically possible and that the WIMP is a scalar or a fermion [23, 61, 62]. The calculation uses the nuclear form factor $f_N = 0.308 \pm 0.018$ [63]. The excluded $\sigma_{\text{WIMP-}N}$ range down to 2×10^{-45} cm^2 in the scalar WIMP scenario. In the fermion WIMP case, the effective coupling is reduced by m_H^2 [29], excluding $\sigma_{\text{WIMP-}N}$ down to 10^{-46} cm^2. While the ATLAS exclusion limits extend to $m_{\text{WIMP}} < 1$ GeV, that

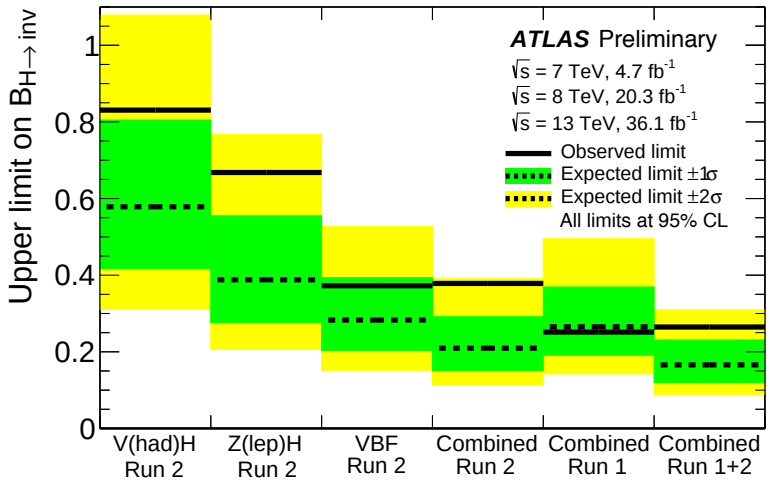

Figure 2: The observed and expected upper limits on $\mathcal{B}_{H\to\text{inv}}$ at 95% CL from direct searches for invisible decays of the 125 GeV Higgs boson and statistical combinations.

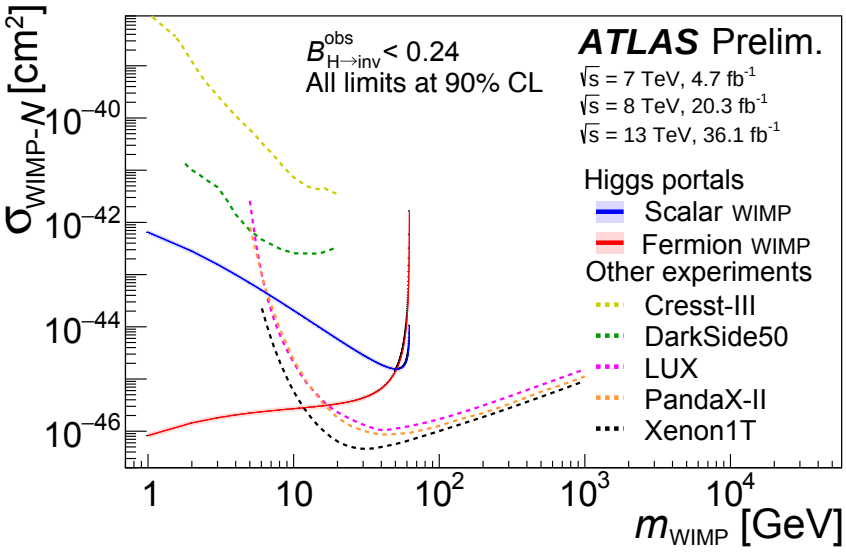

Figure 3: Comparison of the upper limits at 90% CL from direct detection experiments [55–59] on the spin-independent WIMP-nucleon scattering cross section to the observed exclusion limits from this analysis, assuming that the DM particle is either a scalar or a fermion. The regions above the limit contours are excluded in the range shown in the plot.

region is subject to uncertainties in the modelling the nuclear recoil and is therefore not shown explicitly in Figure 3.

In summary, direct searches for invisible Higgs boson decays using up to 36.1 fb^{-1} of pp collision data at $\sqrt{s} = 13$ TeV recorded in 2015 and 2016 in the VBF [33], ZH [34], and VH [35] topologies are statistically combined assuming SM-like Higgs boson production, and an upper limit on the invisible Higgs branching ratio of $\mathcal{B}_{H\to\text{inv}} < 0.38$ ($0.21^{+0.08}_{-0.06}$) is observed (expected) at 95% CL. A statistical combination of this result with the combination of direct $H \to$ inv searches using up to 4.7 fb^{-1} of pp collision data at

$\sqrt{s} = 7$ TeV and up to 20.3 fb^{-1} at 8 TeV collected in Run 1 of the LHC [32] yields an observed (expected) upper limit of $\mathcal{B}_{H\to\text{inv}} < 0.26$ ($0.17^{+0.07}_{-0.05}$) at 95% CL. The combined Run 1+2 result is translated into upper limits on the WIMP–nucleon scattering cross section for Higgs portal models. The derived limits range down to 2×10^{-45} cm^2 in the scalar and 10^{-46} cm^2 in the fermion WIMP scenarios, highlighting the complementarity of DM searches at the LHC and direct detection experiments.

References

[1] Planck Collaboration, *Planck 2018 results. I. Overview and the cosmological legacy of Planck*, (2018), arXiv: 1807.06205 [astro-ph.CO].

[2] WMAP Collaboration, *Nine-Year Wilkinson Microwave Anisotropy Probe (WMAP) Observations: Cosmological Parameter Results*, Astrophys. J. Suppl. **208** (2013) 19, arXiv: 1212.5226 [astro-ph.CO].

[3] A. Boveia and C. Doglioni, *Dark Matter Searches at Colliders*, Ann. Rev. Nucl. Part. Sci. **68** (2018) 429, arXiv: 1810.12238 [hep-ex].

[4] G. Bertone, D. Hooper, and J. Silk, *Particle dark matter: Evidence, candidates and constraints*, Phys. Rept. **405** (2005) 279, arXiv: hep-ph/0404175.

[5] J. L. Feng, *Dark Matter Candidates from Particle Physics and Methods of Detection*, Ann. Rev. Astron. Astrophys. **48** (2010) 495, arXiv: 1003.0904 [astro-ph.CO].

[6] V. Trimble, *Existence and Nature of Dark Matter in the Universe*, Ann. Rev. Astron. Astrophys. **25** (1987) 425.

[7] H. Goldberg, *Constraint on the Photino Mass from Cosmology*, Phys. Rev. Lett. **50** (1983) 1419, Erratum: Phys. Rev. Lett. **103** (2009) 099905.

[8] J. R. Ellis, J. S. Hagelin, D. V. Nanopoulos, K. A. Olive, and M. Srednicki, *Supersymmetric Relics from the Big Bang*, Nucl. Phys. B **238** (1984) 453.

[9] G. Jungman, M. Kamionkowski, and K. Griest, *Supersymmetric dark matter*, Phys. Rept. **267** (1996) 195, arXiv: hep-ph/9506380.

[10] G. Steigman and M. S. Turner, *Cosmological constraints on the properties of weakly interacting massive particles*, Nucl. Phys. B **253** (1985) 375.

[11] R. J. Scherrer and M. S. Turner, *On the relic, cosmic abundance of stable, weakly interacting massive particles*, Phys. Rev. D **33** (1986) 1585, [Erratum: Phys. Rev. D **34** (1986) 3263].

[12] D. Abercrombie et al., *Dark Matter Benchmark Models for Early LHC Run-2 Searches: Report of the ATLAS/CMS Dark Matter Forum*, (2015), arXiv: 1507.00966 [hep-ex].

[13] ATLAS Collaboration, *Observation of a new particle in the search for the Standard Model Higgs boson with the ATLAS detector at the LHC*, Phys. Lett. B **716** (2012) 1, arXiv: 1207.7214 [hep-ex].

[14] CMS Collaboration, *Observation of a new boson at a mass of 125 GeV with the CMS experiment at the LHC*, Phys. Lett. B **716** (2012) 30, arXiv: 1207.7235 [hep-ex].

[15] I. Antoniadis, M. Tuckmantel, and F. Zwirner, *Phenomenology of a leptonic goldstino and invisible Higgs boson decays*, Nucl. Phys. **707** (2005) 215, arXiv: hep-ph/0410165 [hep-ph].

[16] N. Arkani-Hamed, S. Dimopoulos, G. R. Dvali, and J. March-Russell, *Neutrino masses from large extra dimensions*, Phys. Rev. D **65** (2001) 024032, arXiv: hep-ph/9811448 [hep-ph].

[17] A. Datta, K. Huitu, J. Laamanen, and B. Mukhopadhyaya,
Invisible Higgs in theories of large extra dimensions, Phys. Rev. D **70** (2004) 075003,
arXiv: hep-ph/0404056 [hep-ph].

[18] S. Kanemura, S. Matsumoto, T. Nabeshima, and N. Okada,
Can WIMP Dark Matter overcome the Nightmare Scenario? Phys. Rev. D **82** (2010) 055026,
arXiv: 1005.5651 [hep-ph].

[19] A. Djouadi, O. Lebedev, Y. Mambrini, and J. Quevillon,
Implications of LHC searches for Higgs–portal dark matter, Phys. Lett. B **709** (2012) 65,
arXiv: 1112.3299 [hep-ph].

[20] A. Djouadi, A. Falkowski, Y. Mambrini, and J. Quevillon,
Direct Detection of Higgs-Portal Dark Matter at the LHC, Eur. Phys. J. C **73** (2013) 2455,
arXiv: 1205.3169 [hep-ph].

[21] R. E. Shrock and M. Suzuki, *Invisible Decays of Higgs Bosons*, Phys. Lett. B **110** (1982) 250.

[22] D. Choudhury and D. P. Roy, *Signatures of an invisibly decaying Higgs particle at LHC*,
Phys. Lett. B **322** (1994) 368, arXiv: hep-ph/9312347 [hep-ph].

[23] O. J. P. Eboli and D. Zeppenfeld, *Observing an invisible Higgs boson*,
Phys. Lett. B **495** (2000) 147, arXiv: hep-ph/0009158 [hep-ph].

[24] H. Davoudiasl, T. Han, and H. E. Logan,
Discovering an invisibly decaying Higgs at hadron colliders, Phys. Rev. D **71** (2005) 115007,
arXiv: hep-ph/0412269 [hep-ph].

[25] R. M. Godbole, M. Guchait, K. Mazumdar, S. Moretti, and D. P. Roy,
Search for 'invisible' Higgs signals at LHC via associated production with gauge bosons,
Phys. Lett. B **571** (2003) 184, arXiv: hep-ph/0304137 [hep-ph].

[26] D. Ghosh, R. Godbole, M. Guchait, K. Mohan, and D. Sengupta,
Looking for an Invisible Higgs Signal at the LHC, Phys. Lett. B **725** (2013) 344,
arXiv: 1211.7015 [hep-ph].

[27] G. Belanger, B. Dumont, U. Ellwanger, J. F. Gunion, and S. Kraml,
Status of invisible Higgs decays, Phys. Lett. B **723** (2013) 340, arXiv: 1302.5694 [hep-ph].

[28] D. Curtin et al., *Exotic decays of the 125 GeV Higgs boson*, Phys. Rev. D **90** (2014) 075004,
arXiv: 1312.4992 [hep-ph].

[29] ATLAS Collaboration, *Search for invisible decays of a Higgs boson using vector-boson fusion in pp collisions at* $\sqrt{s} = 8$ *TeV with the ATLAS detector*, JHEP **01** (2016) 172,
arXiv: 1508.07869 [hep-ex].

[30] ATLAS Collaboration,
Search for Invisible Decays of a Higgs Boson Produced in Association with a Z Boson in ATLAS,
Phys. Rev. Lett. **112** (2014) 201802, arXiv: 1402.3244 [hep-ex].

[31] ATLAS Collaboration,
Search for invisible decays of the Higgs boson produced in association with a hadronically decaying vector boson in pp collisions at $\sqrt{s} = 8$ *TeV with the ATLAS detector*,
Eur. Phys. J. C **75** (2015) 337, arXiv: 1504.04324 [hep-ex].

[32] ATLAS Collaboration, *Constraints on new phenomena via Higgs boson couplings and invisible decays with the ATLAS detector*, JHEP **11** (2015) 206, arXiv: 1509.00672 [hep-ex].

[33] ATLAS Collaboration, *Search for invisible Higgs boson decays in vector boson fusion at* $\sqrt{s} = 13$ *TeV with the ATLAS detector*, (2018), arXiv: 1809.06682 [hep-ex].

[34] ATLAS Collaboration, *Search for an invisibly decaying Higgs boson or dark matter candidates produced in association with a Z boson in pp collisions at* $\sqrt{s} = 13$ *TeV with the ATLAS detector*, Phys. Lett. B **776** (2018) 318, arXiv: 1708.09624 [hep-ex].

[35] ATLAS Collaboration,
Search for dark matter in events with a hadronically decaying vector boson and missing transverse momentum in pp collisions at $\sqrt{s} = 13$ *TeV with the ATLAS detector*,
JHEP **10** (2018) 180, arXiv: 1807.11471 [hep-ex].

[36] ATLAS Collaboration, *The ATLAS Experiment at the CERN Large Hadron Collider*,
JINST **3** (2008) S08003.

[37] M. Capeans et al., *ATLAS Insertable B-Layer Technical Design Report*, ATLAS-TDR-19 (2010), URL: http://cds.cern.ch/record/1291633.

[38] ATLAS Collaboration, *ATLAS Insertable B-Layer Technical Design Report Addendum*, ATLAS-TDR-19-ADD-1 (2012), URL: http://cds.cern.ch/record/1451888.

[39] CMS Collaboration, *Search for invisible decays of a Higgs boson produced through vector boson fusion in proton-proton collisions at* $\sqrt{s} = 13$ *TeV*, Submitted to: Phys. Lett. (2018), arXiv: 1809.05937 [hep-ex].

[40] CMS Collaboration, *Search for new physics in events with a leptonically decaying Z boson and a large transverse momentum imbalance in proton–proton collisions at* $\sqrt{s} = 13$ *TeV*,
Eur. Phys. J. **C78** (2018) 291, arXiv: 1711.00431 [hep-ex].

[41] CMS Collaboration, *Search for new physics in final states with an energetic jet or a hadronically decaying W or Z boson and transverse momentum imbalance at* $\sqrt{s} = 13$ TeV,
Phys. Rev. **D97** (2018) 092005, arXiv: 1712.02345 [hep-ex].

[42] CMS Collaboration,
Searches for invisible decays of the Higgs boson in pp collisions at $\sqrt{s} = 7$, *8, and 13 TeV*,
JHEP **02** (2017) 135, arXiv: 1610.09218 [hep-ex].

[43] CMS Collaboration, *Search for invisible decays of Higgs bosons in the vector boson fusion and associated ZH production modes*, Eur. Phys. J. **C74** (2014) 2980, arXiv: 1404.1344 [hep-ex].

[44] M. Cacciari, G. P. Salam, and G. Soyez, *The anti-k_t jet clustering algorithm*, JHEP **04** (2008) 063, arXiv: 0802.1189 [hep-ph].

[45] D. Krohn, J. Thaler, and L.-T. Wang, *Jet trimming*, JHEP **02** (2010) 084, arXiv: 0912.1342 [hep-ph].

[46] ATLAS Collaboration, *Jet mass reconstruction with the ATLAS Detector in early Run 2 data*, ATLAS-CONF-2016-035, 2016, URL: https://cds.cern.ch/record/2200211.

[47] G. Cowan et al., *Asymptotic formulae for likelihood-based tests of new physics*, Eur. Phys. J. C **71** (2011) 1554, [Erratum: Eur. Phys. J. C **73** (2013) 2501], arXiv: 1007.1727 [physics.data-an].

[48] W. Verkerke and D. P. Kirkby, *The RooFit toolkit for data modeling*, eConf **C0303241** (2003) MOLT007, arXiv: physics/0306116 [physics].

[49] L. Moneta et al., *The RooStats Project*, (2010), arXiv: 1009.1003 [physics.data-an].

[50] A. L. Read, *Presentation of search results: the CL_s technique*, J. Phys. G **28** (2002) 2693.

[51] ATLAS Collaboration, *Jet energy measurement and its systematic uncertainty in proton–proton collisions at $\sqrt{s}$ = 7 TeV with the ATLAS detector*, Eur. Phys. J. C **75** (2015) 17, arXiv: 1406.0076 [hep-ex].

[52] ATLAS Collaboration, *Jet energy scale measurements and their systematic uncertainties in proton–proton collisions at $\sqrt{s}$ = 13 TeV with the ATLAS detector*, Phys. Rev. D **96** (2017) 072002, arXiv: 1703.09665 [hep-ex].

[53] I. W. Stewart and F. J. Tackmann, *Theory Uncertainties for Higgs and Other Searches Using Jet Bins*, Phys. Rev. D **85** (2012) 034011, arXiv: 1107.2117 [hep-ph].

[54] L. Lyons, D. Gibaut, and P. Clifford, *How to Combine Correlated Estimates of a Single Physical Quantity*, Nucl. Instrum. Meth. **A270** (1988) 110.

[55] F. Petricca et al., "First results on low-mass dark matter from the CRESST-III experiment," *15th International Conference on Topics in Astroparticle and Underground Physics (TAUP 2017) Sudbury, Ontario, Canada, July 24-28, 2017*, 2017, arXiv: 1711.07692 [astro-ph.CO].

[56] D. S. Akerib et al., *Results from a search for dark matter in the complete LUX exposure*, Phys. Rev. Lett. **118** (2017) 021303, arXiv: 1608.07648 [astro-ph.CO].

[57] X. Cui et al., *Dark Matter Results From 54-Ton-Day Exposure of PandaX-II Experiment*, Phys. Rev. Lett. **119** (2017) 181302, arXiv: 1708.06917 [astro-ph.CO].

[58] E. Aprile et al., *Dark Matter Search Results from a One Ton-Year Exposure of XENON1T*, Phys. Rev. Lett. **121** (2018) 111302, arXiv: 1805.12562 [astro-ph.CO].

[59] P. Agnes et al., *Low-Mass Dark Matter Search with the DarkSide-50 Experiment*, Phys. Rev. Lett. **121** (2018) 081307, arXiv: 1802.06994 [astro-ph.HE].

[60] B. Patt and F. Wilczek, *Higgs-field portal into hidden sectors*, (2006), arXiv: hep-ph/0605188 [hep-ph].

[61] P. J. Fox, R. Harnik, J. Kopp, and Y. Tsai, *Missing Energy Signatures of Dark Matter at the LHC*, Phys. Rev. D **85** (2012) 056011, arXiv: 1109.4398 [hep-ph].

[62] A. De Simone, G. F. Giudice, and A. Strumia, *Benchmarks for Dark Matter Searches at the LHC*, JHEP **06** (2014) 081, arXiv: 1402.6287 [hep-ph].

[63] M. Hoferichter, P. Klos, J. Menéndez, and A. Schwenk, *Improved limits for Higgs-portal dark matter from LHC searches*, Phys. Rev. Lett. **119** (2017) 181803, arXiv: 1708.02245 [hep-ph].